16

Titanate Nanotubes as a Versatile Platform for Nanomedicine

Julien Boudon, Anne-Laure Papa, Jérémy Paris and Nadine Millot

Laboratoire Interdisciplinaire Carnot de Bourgogne (ICB), UMR 6303 CNRS-Université de Bourgogne, BP 47870, F-21078, Dijon Cedex, France.

Outline:

Introduction

Titanate nanotubes (TiONts) have received more and more attention [1] since their pioneering hydrothermal synthesis [2]. Recently they have been considered for biomedical applications [3, 4] but not yet as carriers of therapeutic molecules. The synthesis of TiONts with a controlled morphology has been reported [5, 6] and the studies have demonstrated that TiONts were internalized by cells without inducing cytotoxicity [7, 8]. Nevertheless, prior to their use as carriers, it was necessary to determine TiONt biodistribution which has not been reported till date.
In this chapter, the preparation will be first described then the surface modification of TiONts will be exposed; once the TiONt surface is prepared molecules of interest can be grafted such as probes for optical imaging (OI) or macrocyclic chelating agents for the loading of radionuclides to allow nuclear imaging (SPECT, PET), the latter will be developed in the third part along with magnetic properties that can be implemented on TiONts by the grafting of superparamagnetic iron oxide (SPIO) nanoparticles [9]. The fourth and last part will present TiONts themselves or the combination of TiONts with therapeutic molecules. Thereby this chapter covers the development of a novel versatile theranostic (for both therapeutic and diagnostic applications) TiONt-based nanomaterial for nanomedicine.

The preparation of titanate nanotubes and their characterization

Titanate nanotubes can be obtained *via* two methods: first by electrochemical treatment of titanium foil, where tubes grow from the surface by anodization [10] and which leads to nanotubes with a "large" diameter (typically > 25 nm, often 100 nm) [10]; and secondly by hydrothermal treatment [2] which leads to a smaller diameter (around 10 nm). In both cases their length can reach a few hundred nanometers, even the micrometer size in the second case. The TiONts described in this chapter have all been synthesized by hydrothermal treatment of TiO_2 powder.

Titanate nanotubes obtained by anodization

Titanate nanotubes can be obtained from electrochemical treatments (Figure 16.1): an oxidation reaction of a metallic titanium substrate under a specific set of environmental conditions leading to self-organized TiO_2 nanotube layers [11]. Afterwards, TiO_2 nanotubes can be converted into perovskite oxide such as $PbTiO_3$, $BaTiO_3$ or $SrTiO_3$ by hydrothermal treatment in the presence of the corresponding precursor solution. This yields interesting materials for piezoelectric or ferroelectric applications.
In this case, the TiO_2 nanotube growth is controlled by the applied voltage: for example Hashishin *et al.* showed that for a 5h experiment, the growth rate was 321 nm/V in length and 2.33 nm/V in inner diameter resulting in 12-µm-long and 110-nm-inner-diameter nanotubes [12].

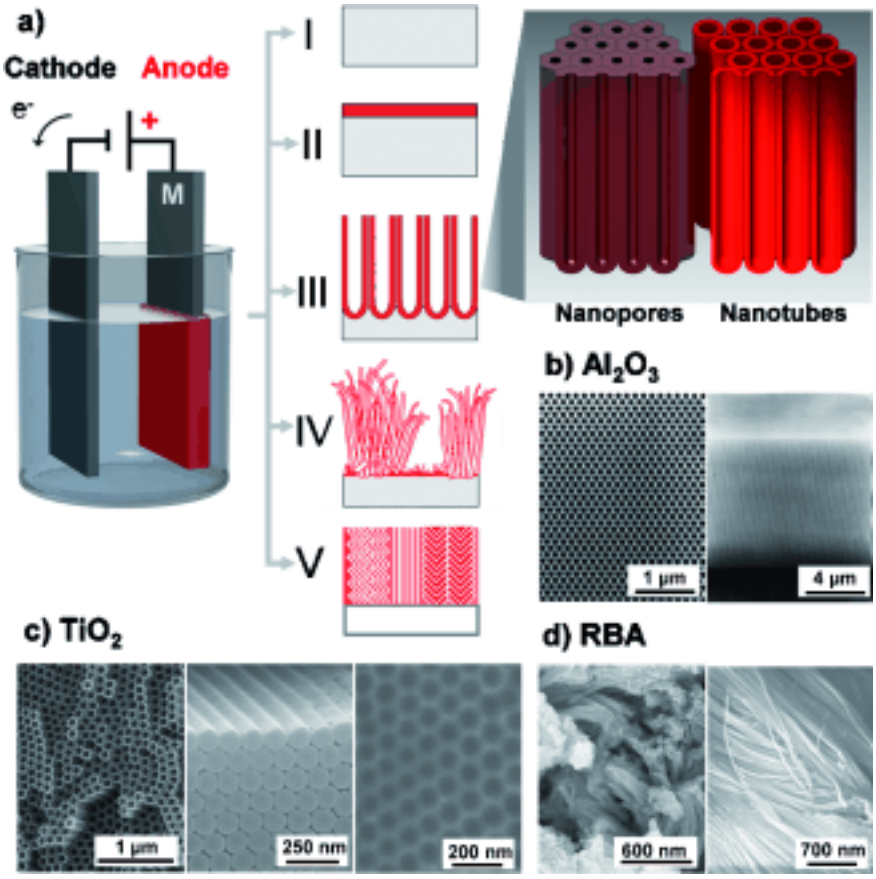

FIGURE 16.1
The electrochemical anodization process and possible anodic morphologies: a) the different phases of anodization process, b) highly ordered nanoporous alumina, c) highly ordered TiO_2 nanotubes, d) disordered TiO_2 nanotubes obtained by rapid breakdown anodization (RBA). Reprinted with permission from Ref. [11]. Copyright 2011 Wiley

However, only a few studies involving anodized nanotubular titanium mentioned their use for biomedical applications. For example, Yao and Webster had an interesting approach by loading penicillin-based antibiotics for prolonged delivery [13]. Still, if these micrometer-sized anodized nanotubes can be used at the surface of titanium implant, they cannot be considered for *in vivo* injection. Indeed large microsized particles are filtrated mechanically by sinusoids and cleared by the reticuloendothelial system (RES) of liver and spleen [14]. In addition, smaller titanate nanotubes could be synthetized by hydrothermal synthesis.

Hydrothermal synthesis of titanate nanotubes

Titanate nanotubes are obtained by the hydrothermal treatment of TiO_2 precursor (anatase [15], rutile [16], both [17] or amorphous [18]) in strongly basic conditions (from 5 to 10 $mol.L^{-1}$ NaOH). Temperature range typically between 100 and 180°C and reaction time ranging from 20 to 72 h have been used in their preparation (lower and higher temperatures are possible depending on the NaOH

concentration used). The time of reaction can be reduced to a few hours with presonication of the reaction mixture [19], however, a 100% yield is difficult to reach [5, 15, 20]. Nanosheets are produced as byproducts of the reaction and they represent about 10% of the batch with optimal conditions of synthesis [5]. It has been shown that the amount of byproducts produced can be quantified from the XRD (X-Ray Diffraction) patterns of the samples [5]. Complex schemes and morphology diagrams have been proposed, trying to emphasize the sensitive nature of the synthesis (Figure 16.2) [6, 21]. The main parameters that must be controlled to yield a majority of tubular-shaped titanate nanomaterials have been extensively investigated [5, 22, 23]. Titanate nanotubes' synthesis is highly sensitive to reaction conditions and their yield relies on various parameters such as precursor phase, NaOH concentration, reaction time, mixing mode and speed. Indeed, a slight variation of these parameters can preferentially lead to the formation of a majority of titanate nanoribbons or nanosheets rather than nanotubes. Our studies have shown that the optimal parameters are the following ones: rutile precursor, 10 mol.L^{-1} NaOH, 36 hours of hydrothermal treatment, magnetic stirring at 120 rpm [5]. An acidic post treatment (to the hydrothermal synthesis) was initially described by Kasuga *et al.* as a key parameter of the nanotubes formation. Later in literature, it has been shown that acid washings were not required to obtain nanotubes [24], however this treatment has been described for increasing the porosity (consequently the specific surface) and to modulate the composition (Na^+ substitution by H^+) of the already formed nanotubes [25, 26].

The formation mechanism of titanate nanotubes is still a matter of debate. Several phenomena are discussed in literature: the dissolution of the precursor crystallites in bulk followed by their precipitation into nanosheets which then curl into nanotubes [27], and an energy-dependent curling process of nanosheets first exfoliated from the particle block [28, 29]. The kinetics of their formation has also been studied and demonstrated to be precursor size dependent [30]. TiONt formation mechanism has been extensively reviewed by Bavykin, Walsh and colleagues [31, 32].

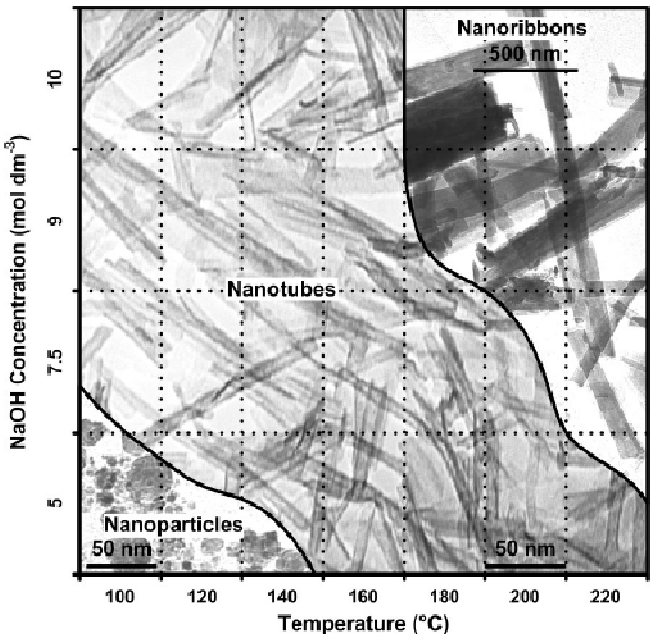

FIGURE 16.2
Morphological phase diagram ([NaOH],T) proposed by Morgan *et al.* [6, 15, 33] Reprinted with permission from Ref. [6]. Copyright 2008 American Chemical Society

Titanate nanotubes features and characterizations

Titanate nanotubes, whose phase composition is $\mathbf{Na_xH_{2-x}Ti_nO_{2n+1} \cdot yH_2O}$, are rolled up like a spiral (contrary to carbon nanotubes the walls of which are concentric). They have an inner cavity (around 4nm, Figure 16.3a) and they are defined by two crystal lattices: 0.7 nm perpendicular to their longitudinal axis (and also the distance between two consecutive walls) and 0.36 nm at 76° from the main axis [33, 34]. The size characteristics (such as length, inner diameter and outer diameter distributions) may vary depending on the synthesis parameters. It has been shown that titanate nanotubes can display asymmetry in the number of walls that they have (Figure 16.3b). Beyond their morphology, the interesting feature developed by these tubes is their highly increased specific surface area (Figure 16.3c) in comparison to their spherical TiO_2 precursors. In the first published synthesis of nanotubes [2], Kasuga *et al.* have reported a 400 $m^2.g^{-1}$ surface area. The surface of these tubes is also interestingly covered with hydroxyl groups, which allow anchoring for further functionalization (described in part 2). The ζ-potential of TiONts is negative after synthesis followed by washing till pH 6 and this is due to these hydroxyl groups. It has been shown that their isoelectric point (IEP) is 3.6 [9]. After synthesis, nanotubes appear aggregated (micrometer size) but a post-functionalization by polymers (PolyEthylenImine (PEI) [7, 35], PolyEthylene Glycol (PEG) [35], Poly(ε-CaproLactone (PCL) [36]) is able to disperse and stabilize their suspension. This step is also essential to improve the circulation properties of the particles in the blood stream for nanovectorization purposes and to improve their biocompatibility in the case of PEGylation.

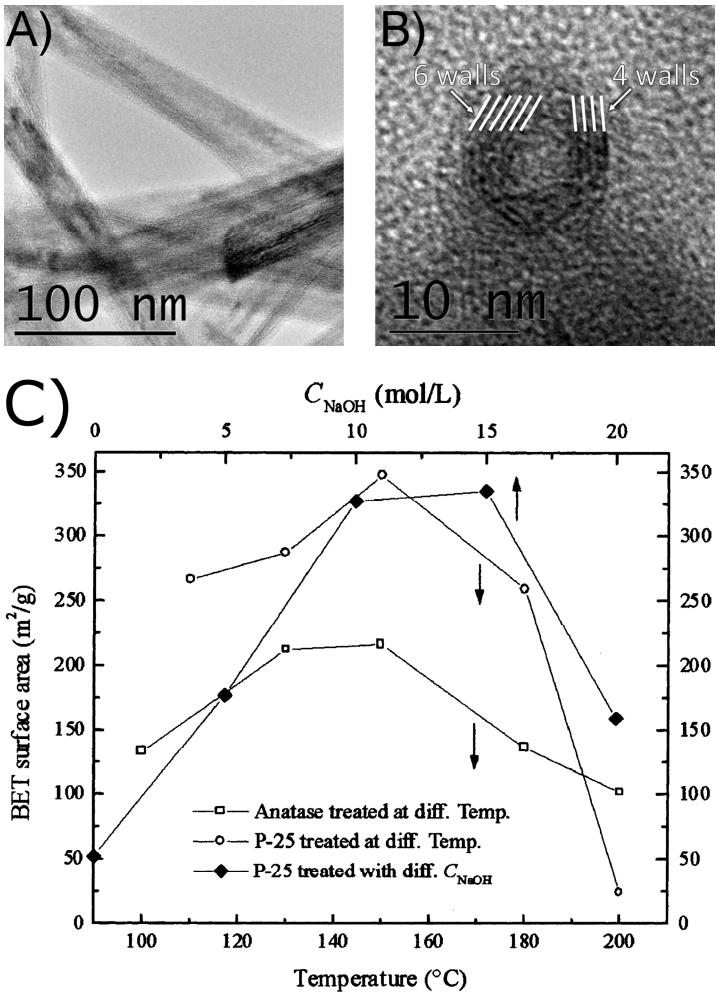

FIGURE 16.3
TiONts: (A) TEM image, (B) HRTEM image depicting wall asymmetry and (C) specific surface area of titanate nanoparticles synthesized by hydrothermal treatment from anatase TiO_2 and P25 (Degussa) in 10 $mol.L^{-1}$ NaOH at various temperature during 24 h and products obtained from P25 with various NaOH concentrations at 110°C. Figure 16.3c is reprinted from Ref. [37], Copyright 2004, with permission from Elsevier

The surface modification of titanate nanotubes

The physicochemical properties of TiONts and more generally speaking nanoparticles (NPs), such as size (*i.e.* hydrodynamic diameter d_H), hydrophobicity, surface charge, will affect the *in vivo* biodistribution and clearance [38]. NPs with d_H below 6 nm can be excreted through the renal route, whereas larger uncoated NPs are more easily recognized and cleared by the liver and phagocytic cells of the reticuloendothelial system (RES) [39] and thus excreted through the hepatobiliary route. Rapid clearance can be partially alleviated by adding polymer coatings, like poly(ethylene glycol) (PEG).

Surface charge also plays a crucial role in the rapid elimination of NPs from the blood by the RES uptake because surface charge can increase d_H of NPs by non-specific adsorption of plasma protein, which increases opsonization, *i.e.* removal of NPs by RES macrophages. In the meantime, NPs have to be in the size range of a few hundreds of nm in order to target and stay into tumors in case of NP-mediated targeting therapy: the enhanced permeability and retention (EPR) effect is harnessed by an acute control of the size and surface chemical groups of NPs [39].
After synthesis, TiONts – and more generally speaking metal oxides – undergo agglomeration because of the hydroxyl functions present at their surface that create neither sufficient electrostatic nor enough steric repulsion for stable colloidal suspensions. In order to circumvent the relatively low reactivity and/or the lack of mild coupling conditions involving hydroxyl functions, surface modifications have been developed to adapt to a wide majority of molecules of interest for imaging and/or therapy. The aim is to tune the TiONt surface by converting initial OH groups into amines, carboxylic acids or thiol functions capable to react with imaging probes or biological molecules bearing activated ester, amine or maleimide moieties. These modifications can not only enhance the reactivity towards molecules of interest but also increase the electrostatic repulsion *via* ammonium (positive charges) or carboxylates (negative charges). Surface modification by silane and phosphonate derivatives are described in the following paragraphs.

TiONt modification by silane derivatives

Amino- and mercapto-alkoxysilane derivatives are used to modify TiONt surfaces to introduce amine (Figure 16.4) or thiol groups (not shown). It is a convenient organic approach to the surface modification of TiONts [40, 41] as numerous derivatives are commercially available including various chemical groups borne on different chain-length alkanes.

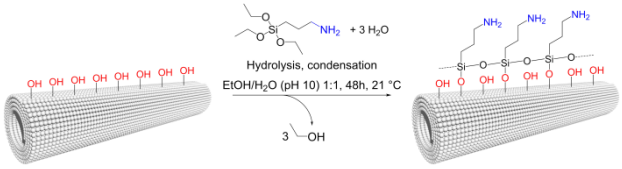

FIGURE 16.4
Example of surface modification of TiONts by an *ω*-aminosilane derivative to yield amino-functionalized TiONts

Short carbon chains are preferred so that the implemented functions do not imbed into the organic layer. For example, 3-aminopropyltriethoxysilane (three-carbon chain) was used to bring amine functions to the surface of iron oxides nanoparticles [42, 43]. The reaction of silane on metal oxides occurs in three consecutive steps under mild temperature and reduced pressure conditions [44]: i) silanes are first hydrolyzed into silanols; ii) silanols form polysiloxanol films; iii) polysiloxanol films are condensed on the metal oxide surface (briefly illustrated on Figure 16.4). It is a convenient way to yield stable surface-modified titanate nanotubes exhibiting readily available chemical functions (NH_2, COOH, SH) that are conventionally encountered in biochemistry (*e.g.* amines and carboxylic acids forming amides, thiols and maleimides forming thioethers).

The titanate nanohybrids formed are characterized by a series of techniques to assert the presence of the grafted silane derivatives: thermogravimetric analysis (TGA), X-ray Photoelectron Spectroscopy (XPS), Fourier-transformed Infrared Spectroscopy (FTIR), elemental analysis (EA, also referred to as

CHNX analyses), Energy-dispersive X-ray spectroscopy (EDS) associated with transmission electron microscopy (TEM) observations, ζ-potential measurements according to pH variations.

TiONt modification by phosphonate derivatives

Another suitable approach to the surface modification of TiONts implies phosphonate derivatives [45] to introduce *e.g.* carboxylic acids groups. A recent review clarifies the interactions of phosphonate derivatives with metal oxide surfaces [45]: contrary to the silane homocondensation before condensation on the metal oxide surface, phosphonates individually condensate on metal oxide surfaces potentially conferring a better stability of the grafted organic layer. Additionally the interaction of phosphonate derivatives, *e.g.* ω-functionalized alkylphosphonate derivatives X–$RPO(OH)_2$, which could involve two (cf. Figure 16.5 as illustration) or three oxygen atoms to coordinate the metal oxide surface depending on the deprotonated phosphonate anion intermediate: mono-deprotonated $RPO_2(OH)^-$ or fully deprotonated RPO_3^{2-}.

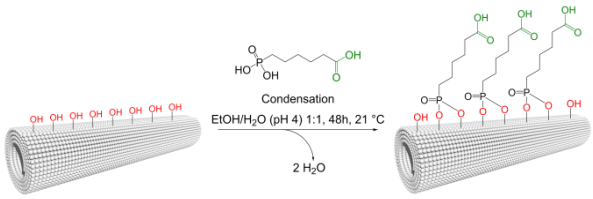

FIGURE 16.5
Example of surface modification of TiONts by an ω-carboxysilane derivative to yield carboxyl-functionalized TiONts

6-phosphonohexanoic acid (PHA) was successfully used to modify TiONt surface. As a consequence TiONt suspensions are more stable after grafting than before (Figure 16.6 left) and even more stable than aminosilane-functionalized TiONts (Figure 16.6 right).

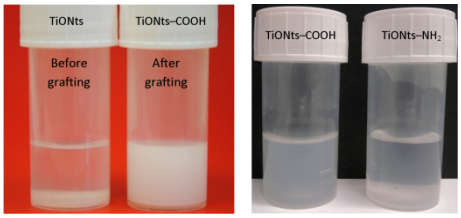

FIGURE 16.6
On the left: result of surface modification of TiONts by 6-phosphonohexanoic (PHA) acid ligands on the suspension stability. On the right: difference between stabilizers (PHA lead to TiONts–COOH and APTES to TiONts–NH_2) on the suspension stability

As an illustration of successful graftings by aminosilanes or phosphonohexanoic acids on TiONts, a selection of characterizations is provided in the following paragraph.

Characterizations of surface-modified TiONts

Despite a low isoelectric point (pH 3.3) and a high value of ζ-potential (approximately -30 mV) in physiological conditions at pH 7.4 (Figure 16.7), bare nanotubes suspensions are not stable. Unfortunately the same phenomenon is observed for APTES-modified TiONts (Figure 16.6), but it is not

the case of PHA-modified TiONt suspensions which are stable during at least 24 h in the same conditions. As shown in Figure 16.7, TiONt surface modification by APTES shifts the isoelectric point towards higher pH values (*ca.* 6.3). However, the surface modification by PHA barely changes the isoelectric point (*ca.* 3.2) as well as ζ-potential at pH 7.4 but increases stabilization (Figure 16.6).

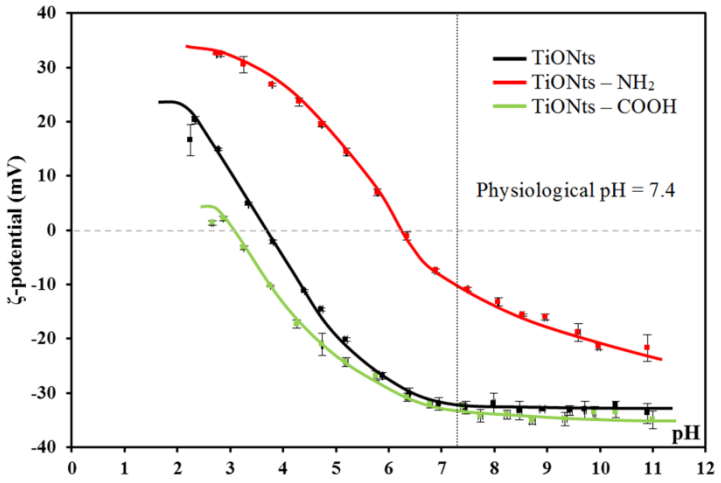

FIGURE 16.7
TiONts, TiONts–NH_2 and TiONts–COOH ζ-potentials according to pH variations measured in 10^{-2} $mol.L^{-1}$ NaCl solution

Significant differences in IsoElectric Points (IEP) and ζ-potentials at pH 7.4 are noticed when bare TiONts and aminosilane-modified TiONts or carboxyphosphonate-modified TiONts are compared (Table 16.1).

TABLE 16.1
TiONts, TiONts–NH_2 and TiONts–COOH isoelectric points (IEP) and ζ-potentials at physiological pH

	IEP	ζ-potential (mV) at pH 7.4
TiONts	3.3 ± 0,2	-32 ± 3
TiONts–NH_2	6.3 ± 0,8	-13 ± 4
TiONts–COOH	3.2 ± 0,3	-35 ± 3

As could be expected from ζ-potential values at pH = 7.4 presented in Table 16.1, TiONts–NH_2 are not stable into physiological medium (pH 7.4 and 0.9 weight% NaCl) or into PBS buffer while TiONts–COOH are stable during at least 24 hours.

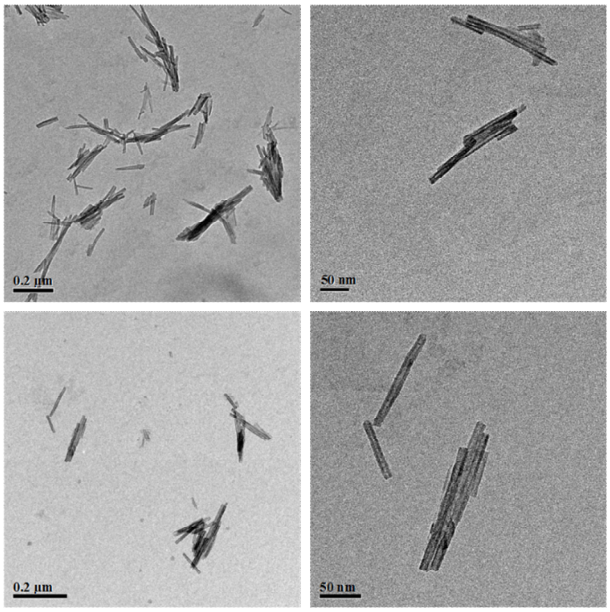

FIGURE 16.8
TiONts–NH_2 (top) and TiONts–COOH (bottom) TEM observations showing small bundles of functionalized TiONts

According to TEM observations (Figure 16.8), the surface modification leads to nm-sized agglomerates of TiONts contrary to the µm-sized agglomerates showed by bare TiONts (not shown in this chapter, see [7] for example).

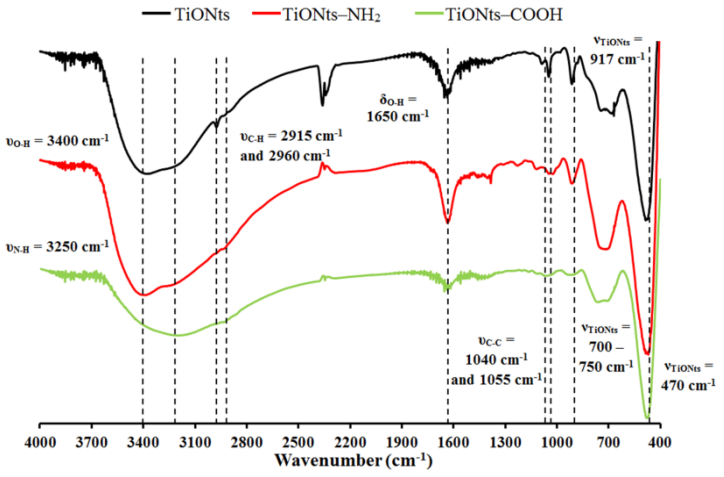

FIGURE 16.9
TiONts, TiONts–NH_2 and TiONts–COOH FTIR spectra

FTIR spectroscopy (Figure 16.9) was also used to characterize TiONts (note that the 2400 cm^{-1} band represents CO_2 pollution): metal oxide hydroxyl groups exhibit vibration bands at 1630 cm^{-1} and 3400

cm^{-1}. TiONt specific vibration modes are located from 470 cm^{-1} to 917 cm^{-1} of which the 700-750 cm^{-1} partial band is still present after grafting.
After grafting, the presence of the APTES ligand carbon chains is confirmed by the appearance of bands at 2915 and 2960 cm^{-1} corresponding to the C–H vibrational modes, N–H vibration bands are located at 3250 cm^{-1} and 1625 cm^{-1} but are combined with that of the adsorbed water. Vibration modes around 1050 cm^{-1} may correspond to the vibrations of C–C bonds but also to the characteristic ones of APTES ligands (Si–O–Si) or PHA ligands (P–O). This difference is not readily observable in the FTIR spectra but suggests the presence of the ligands on the surface of TiONts.

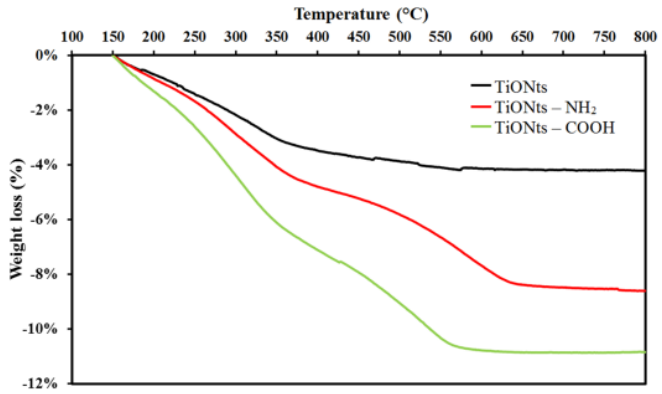

FIGURE 16.10
TiONts, TiONts–NH_2 and TiONts–COOH thermogravimetric analyses

Relative weight losses between 150 °C and 800 °C of surface-modified TiONts are greater than that of bare TiONts suggesting the presence of organic ligands at the nanoparticles surface (Figure 16.10). TiONts–COOH exhibit a greater relative weight loss when compared to that of TiONts–NH_2, which is not surprising since the carbon chain of PHA (6-carbon chain) is heavier than the APTES one (3-carbon chain). Thus the ligand grafting rate of surface-modified TiONts is estimated using the BET specific surface area of the bare TiONts which is (163 ± 25) $m^2.g^{-1}$ determined on ten different TiONt syntheses.

TABLE 16.2
Grafting rates of surface-modified TiONts in the cases of APTES (NH_2) or PHA (COOH) molecules modifications (standard deviations on grafting rates are obtained from repeated experiments)

	Relative weight loss (%)	Molecular weight of leaving species ($g.mol^{-1}$)	Grafting rate ($molecules.nm^{-2}$)
TiONts	3.8	18	(6.0 ± 4.0) OH
TiONts–NH_2	8.0	58	(5.7 ± 0.8) NH_2
TiONts–COOH	10.9	115	(3.1 ± 0.5) COOH

When TiONt samples are analyzed by XPS (Figure 16.11), carbon and oxygen 1s energy levels are decomposed: the C1s level highlights the C–NH_2 bond of APTES-modified TiONts. On the other hand,

the components related to the PHA carbon skeleton on TiONts–COOH are identified as the components corresponding to the C–P and (C=O)–OH bonds. The proportion increase of the C–C/C–H component also reveals the presence of carbon ligands at the surface-modified TiONts.

Decomposition of the modified TiONts O1s energy level emphasizes the emergence of new components. Concerning TiONts–COOH, the component at 529.7 eV corresponds to the oxygen network and the one at 532.2 eV to the (C=O)–OH double bond. The component at 531.0 eV can be attributed to oxygen bonds within phosphonates (P=O/P–O–), but also to the remaining surface hydroxyl. In addition to the presence of the ligands at the surface of TiONts–COOH, sodium Auger electrons are no longer present at 535.0 eV (when compared to bare TiONts). Because the PHA grafting occurs at acidic pH, the sodium ions are thus exchanged with hydrogen ions from the H_2O/EtOH environment.

The XPS analysis of APTES-modified TiONts shows no difference in the decomposition of the O1s energy level. The same components as bare TiONts are observed: (i) the O^{2-} oxygen network component at 529.7 eV, (ii) the OH surface hydroxyls component at 531.5 eV, and (iii) the sodium Auger electrons at 535 eV. The presence of the surface hydroxyls component at 531.5 eV suggests that all surface hydroxyls were not involved in the APTES grafting. The atypical morphology of TiONts as well as an incomplete silane condensation could explain the existence of the surface hydroxyls component after APTES grafting.

The characterizations of TiONt nanohybrids are in correlation with TiONt suspensions observation because surface-modified TiONts appeared more stable when compared to their parent unmodified TiONts (Figure 16.6).

Depending on the post-functionalizing steps reaction conditions, silane-modified TiONts generally lead to unstable suspensions because of isoelectric points (IEP) around pH 7 too close to the pH of physiological conditions (pH 7.4). In that particular case further stabilizing molecules must be grafted to sterically stabilize them. In other cases another approach involving phosphonate derivatives is preferred and will be detailed in the following paragraph.

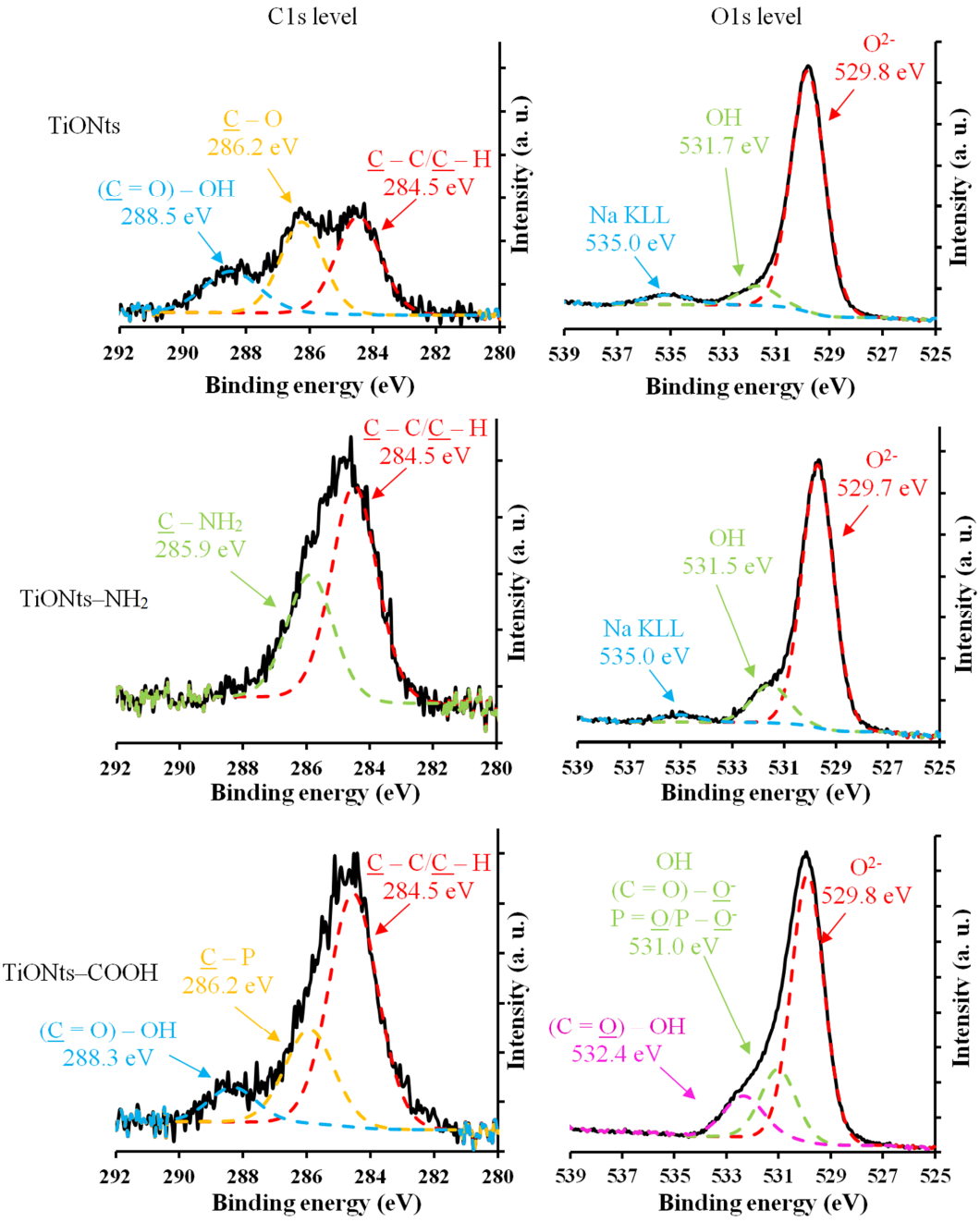

FIGURE 16.11
TiONts, TiONts–NH_2 and TiONts–COOH XPS analyses at C 1s and O 1s energy levels

The grafting on titanate nanotubes with a view to in vivo imaging

One of the major challenges with the use of TiONts for molecular imaging is a covalent grafting of imaging probes to assert the presence of TiONts. This part presents the successful synthetic strategies developed to realize TiONt-based imaging.

Optical imaging

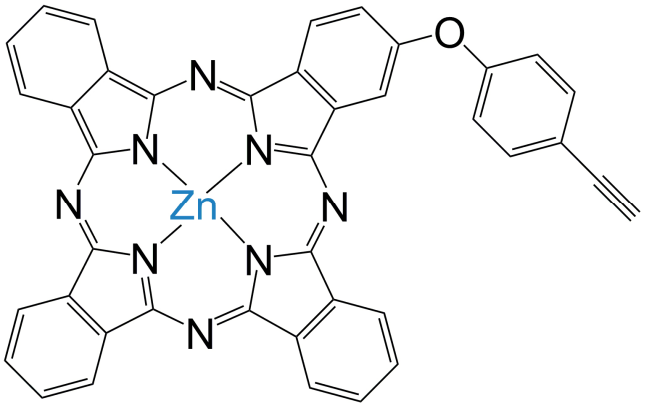

FIGURE 16.12
A zinc phthalocyanine derivative bearing an alkyne ready for coupling by click chemistry on TiONts

The introduction of fluorescence-based optical probes is of great interest for optical imaging. However in the case of *in vivo* optical imaging the absorption of the various tissue and blood components [46] rather limits the use of conventional fluorophores (*e.g.* fluorescein or rhodamine derivatives). Other approaches are developed for *in vivo* optical imaging based on phthalocyanine derivatives [43] (Figure 16.12) the absorption band of which lies in the 650–800 nm region where light penetration in tissues is the deepest.
Phthalocyanine compounds are synthetized by the condensation of four isoindole groups leading to a fully conjugated system capable of high molar extinction coefficients (*e.g.* ε(ZnPc) = 1.85 10^5 $L.mol^{-1}.cm^{-1}$), very low photobleaching – when compared to conventional fluorophores – and high quantum yields. In addition some of the isoindole can be substituted in order to add anchoring possibilities to the macrocycles which forms complexes with a wide variety of metal ions (*e.g.* Zn, Al, Si). Indeed, even if phthalocyanines are analogues of porphyrin macrocycles, they do not exhibit hypsochromic shifts when grafted on nanoparticles [47]. For example, a recent communication used an alkyne moiety on zinc phthalocyanines to run click chemistry on azide-functionalized iron oxide nanoparticles and no wavelength shift was observed (Figure 16.13) [43].

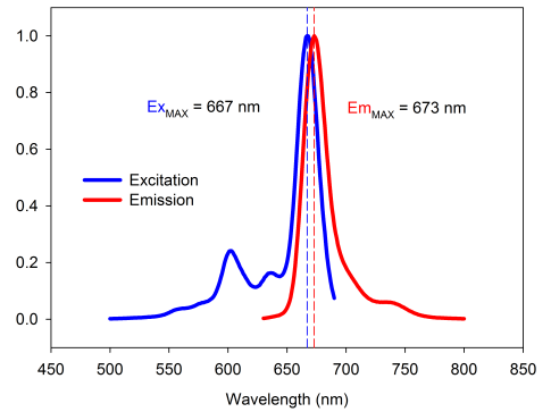

FIGURE 16.13
On the right: fluorescence emission and excitation of phthalocyanine-grafted iron oxide nanoparticles in ethanol

Upon excitation of zinc phthalocyanine-grafted metal oxide nanoparticles at 600 nm in ethanol solution, a fluorescence emission (Figure 16.13) at 673 nm was observed, which is comparable to the fluorescence emission of the parent free zinc phthalocyanine. The results seem to indicate that there is no Aggregation Caused Quenching (ACQ) due to π-stacking and Förster Resonance Energy Transfer (FRET) quenching in the organic solvent. As a consequence phthalocyanine-based nanohybrids are promising candidates for *in vivo* optical imaging.

Nuclear imaging

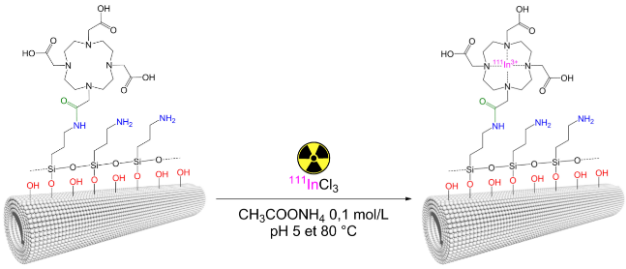

FIGURE 16.14
^{111}In radiolabeling of DOTA-grafted TiONts for SPECT imaging

The grafting of macrocyclic DOTA-based chelators is an elegant way to ensure that the radionuclide chosen for Single Photon Emission Tomography (SPECT) or Positron Emission Tomography (PET) is actually tethered to TiONt carrier. DOTA derivatives grafting, radiolabeling (Figure 16.14) and imaging capabilities is of particular interest to follow TiONt biodistribution.

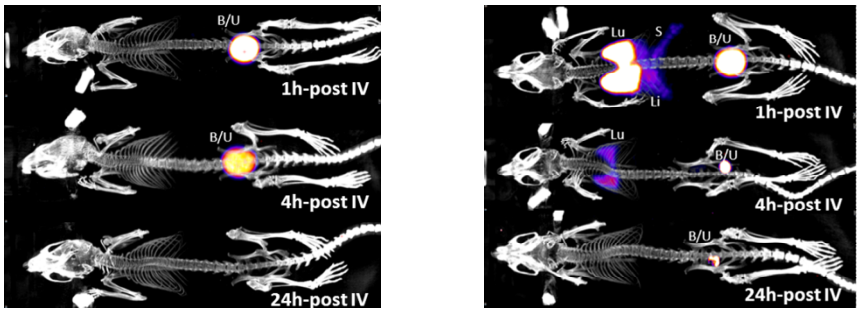

FIGURE 16.15
Reconstructed images of *in vivo* SPECT/CT dual imaging of Swiss nude mice intravenously injected with 15 MBq DOTA[^{111}In] (left panel), TiONts-DOTA[^{111}In] (right panel), at 1 h, 4 h and 24 h post-injection

Just after DOTA-grafted TiONts were radiolabeled by ^{111}In, Swiss nude mice were injected. 1 h after injection the difference between the two compounds is obvious highlighting the success of the functionalization and radiolabeling TiONts-DOTA. Indeed, the free DOTA[^{111}In] compound is rapidly eliminated because the radioactivity is exclusively in the bladder after an hour and it is then removed continuously until total elimination by excretion.
Instead, TiONts–DOTA[^{111}In] flow through the lungs, liver and spleen, but they are also gradually eliminated by excretion through the bladder. At 24 hours, the TiONts–DOTA[^{111}In] are no longer present in the bladder and are most likely be subsequently removed by natural means (no imaging was performed after 24h).

Magnetic resonance imaging

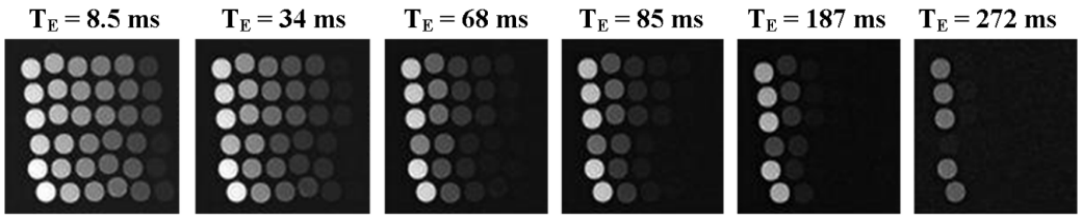

Figure 16.16
T_2-weighted MRI phantoms for six different echo times T_E and for six increasing concentrations (from left to right) of two different samples (in triplicates) of TiONts–SPIO nanocomposites

The combination of TiONts to superparamagnetic iron oxide (SPIO) nanoparticles is an interesting approach for magnetic resonance imaging (MRI) based on inorganic nanomaterials. Indeed SPIO nanoparticles are effective T_2 contrast agents (negative contrast), the synthesis of which is also well-known [9, 48, 49].
Three different pathways were used to obtain TiONts-SPIO nanocomposites: TiONt hydrothermal synthesis in the presence of SPIO nanoparticles, [9] SPIO soft chemistry synthesis in the presence of TiONts and finally co-synthesis of both SPIO and TiONts by hydrothermal synthesis (Figure 16.17).

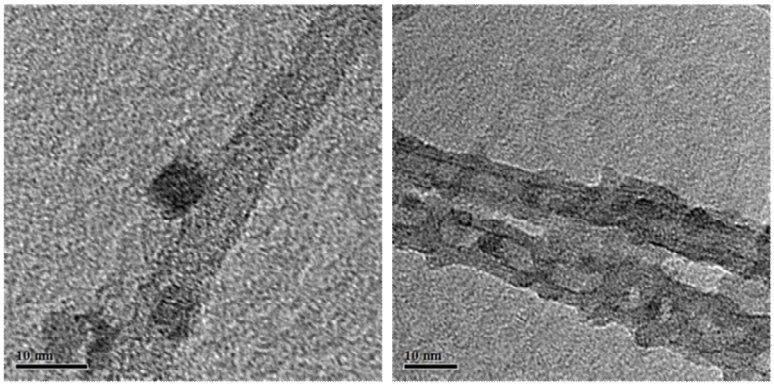

FIGURE 16.17
TEM observations of TiONts–SPIO nanocomposites (Fe/Ti mass ratio is 1:2) obtained by co-synthesis

SuperParamagnetic Iron Oxide (SPIO) nanoparticles grafted onto TiONts allow the resulting nanocomposite to be itself superparamagnetic because of the SPIO crystallite size which is less than 20 nanometers. MRI measurements on acrylamide gels (Figure 16.16), lead to relaxivities comparable to that found in literature [50]. Thus TiONts–SPIO nanocomposites are capable to act as nanocarriers that can be followed by magnetic resonance imaging.

Therapeutic applications of titanate nanotubes

In the biomedical field, titanate nanotubes have been investigated for their use in bone regeneration [51, 52], dopamine detection [53] and molecule vectorization [7, 54]. In this last part of the chapter are presented three examples of TiONts use for therapeutic applications: the first one is the use of TiONts themselves to increase the efficacy of a radiotherapy treatment; the second one is the grafting of docetaxel, a taxane derivative for antitumor activity and the third one is the use of a phthalocyanine derivative for photodynamic therapy (PDT).

TiONts as radiosensitizers

The major challenge in radiation oncology is to exert therapeutic effects on tumor while preventing unwanted effects on normal surrounding tissue. To remedy this limitation, one interesting approach in research so far has been to use nanoparticles able to enhance radiation effects (due to their intrinsic properties [55] or by carrying a radioelement [56]), while focusing the dose on a minimal area of treatment. Indeed, nanoparticles containing a high atomic number (Z) element, such as gold (Z = 79), [55] platinium (Z = 78), [57] gadolinium (Z = 64) [58] and silver (Z = 47), [59] have been attractive for their radiosensitizing effect on tumor cells. Particles under radiation stabilize their energy by both re-radiation photons (photoluminescence phenomenon) and emission of secondary and Auger electrons, thus leading to the generation of Reactive Oxygen Species (ROS). These oxygen species generate DNA double strand breaks and consequently, cause nuclear damage and have deleterious effects on cell survival [60]. Nanoparticles offer a dual advantage as their tunable size and surface-grafting permit the generation of suitable size distributions at which EPR (Enhanced Permeability and Retention) effect can be achieved [61, 62]. The vasculature surrounding the tumor is disorganized and highly permeable while the lymphatic system is defective. These factors taken together lead to the

passive targeting (so called EPR) of the nanoparticle to the tumor site. If nanoparticles are able to increase cell sensitivity to radiation, a minimal dose can be administered and be effective on tumor burden, while remaining safe for surrounding healthy tissues.

Nanoparticle-cell interaction is reported in many reviews [63-73] but the main observation regarding the effect of nanoparticles on cells is the production of reactive oxygen species, leading to oxidative stress. Functionalized and naked nanoparticles have been shown to increase p53 (a tumor suppressor protein) and phospho-p53 expression, as well as leading to Rad51 up-regulation and an increase in γH2AX [8, 65]. All these proteins are involved in the DNA repair pathway. Nanoparticles have also been shown to induce cell cycle arrest [8, 74]. Based on their cytotoxic effects, targeted nanoparticles could then offer new avenues in cancer research [75].

Though titanium is not a heavy metal (Z = 22), its potential as radiosensitizer has been considered as other low atomic number elements like calcium (Z = 20) and phosphorus (Z = 15) have demonstrated DNA damage incidences after X-ray exposure [76, 77]. Also, titanate nanotubes were a prime candidate for this application as their internalization ability in cells has been demonstrated to be higher than their spherical counterparts [7]. Similar enhancement of internalization as a function of physical shape has been observed for organic particles as well [78]. Titanate nanotubes have shown no cytotoxicity when incubated with glioblastoma cell lines (SNB-19 and U87MG) but exert radiosensitization on both cell lines with a significant decrease of the SF_2 parameter (survival fraction of cells at 2 Gy) [8] (Figure 16.18). This effect of TiONts has been validated at low and high doses as confirmed by an increase and decrease respectively of α and β parameters. Biological consequences have been investigated by detection of apoptosis, autophagy and ROS production without concluding that any of these factors could explain the radiosensitization effect of TiONts (in the experimental conditions tested). However, a clear implication of cell cycle impairment has been highlighted. Indeed, DNA damage and repair assessed by γH2AX quantification 1 h and 24 h after irradiation at 2 Gy, with and without TiONts, has demonstrated that TiONts induce a cell accumulation at the G2/M checkpoint [8]. Prior literature has shown that cancer cells are more sensitive to radiation when they are in G2 phase. It has been hypothesized that the observed accumulation of cells at the G2/M checkpoint could be due to TiONt-induced DNA damage, and that this G2/M arrest would subsequently promote the radiation induced therapeutic effect [8]. However further investigation on the effect of TiONts on DNA need to be pursued to clarify the process.

In perspective, if improving the tumor targeting and lowering the radiation dose can be achieved by using selected nanoparticles, a gap still remain in mitigating the bystander effect [60] produced by radiation therapy. The radiation-induced bystander effect are collateral damages produced in surrounding cells due to signaling molecules traveling from irradiated cells to neighboring normal ones. This effect induces genome instability and may contribute to secondary cancers [79]. Small signaling inhibitors delivered with nanoparticles could potentially address this complex issue and offer an additional level of protection to healthy surrounding tissues. To date, the potential of a combined radiosensitizer and a signaling pathway inhibitor has not yet been reported and could offer a synergistic response.

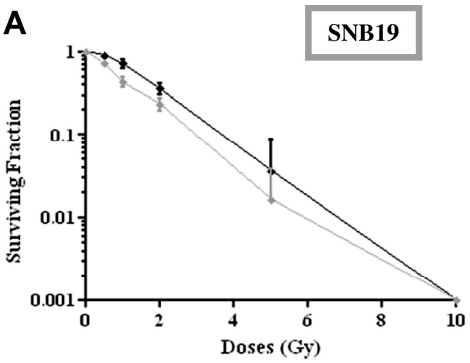

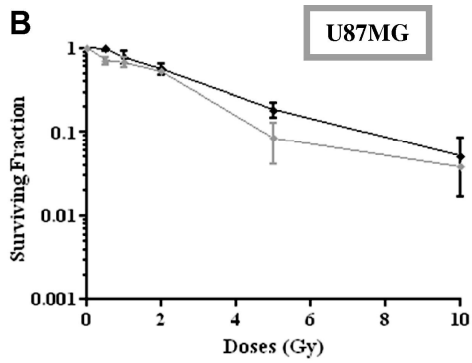

	Without TiONts	1µg/ml TiONts
α	0.12 ± 0.12	0.71 ± 0.16 *
β	0.19 ± 0.02	0.07 ± 0.05 *
SF_2	0.36 ± 0.05	0.18 ± 0.05 *

	Without TiONts	1µg/ml TiONts
α	0.19 ± 0.08	0.38 ± 0.07 *
β	0.03 ± 0.00	0.01 ± 0.01 *
SF_2	0.60 ± 0.08	0.43 ± 0.05 *

FIGURE 16.18
Survival fraction curves obtained from SNB-19 and U87MG showing the effect of X-ray exposure (different doses) without TiONts (control: black curve) or with 1 µg/mL TiONts incubation (grey curve). Radiosensitization parameters (α: initial slope, β: degree of downward curvature and SF2: survival fraction at 2 Gy) were extracted from these curves with the Linear Quadratic model (LQ-model). Reprinted from reference [8], copyright 2013 with permission from Elsevier

Chemotherapy by taxane-grafted TiONts

Docetaxel (DTX) is a clinically well-established anti-mitotic chemotherapy taxane-type drug. Its combination with TiONts is of great interest for tumor treatment, TiONts acting as a drug carrier in case of systemic injection. The grafting strategy of a docetaxel derivative is presented in Figure 16.20 and the results of MTS biological tests on a PC3 human prostate cancer cell line in Figure 16.19.
Preliminary biological results did not show any cytotoxicity for surface-modified TiONts before cytotoxic docetaxel drug molecules were grafted on them (Figure 16.19, green dashed-dotted line) as opposed to free docetaxel having a 4 nM IC50 (Figure 16.19, orange dashed line). In order to have DTX drug covalently bound on TiONts, DTX had to be modified by a crosslinker: modified DTX molecules are 4-fold less toxic (IC50 is increased to *ca*. 20 nM, see Figure 16.19, dark red line) than unmodified docetaxel. The activity of docetaxel grafted directly at the surface of TiONts did not lead to satisfactory IC50 cytotoxicity (not shown) but the introduction of a PEG spacer – between TiONts and docetaxel – decreases the steric bulkiness brought by the proximity of docetaxel molecules on TiONts. Thus PEGylated docetaxel molecules more freely interact with tubulin subunits in microtubules. That is the reason why TiONts-PEG-DTX nanohybrids are considered for further studies on mice xenografted by prostate tumors. The next elaboration steps will notably consist in optimizing the docetaxel grafting rate on TiONts in order to increase treatment efficacy without increasing the nanotube load.

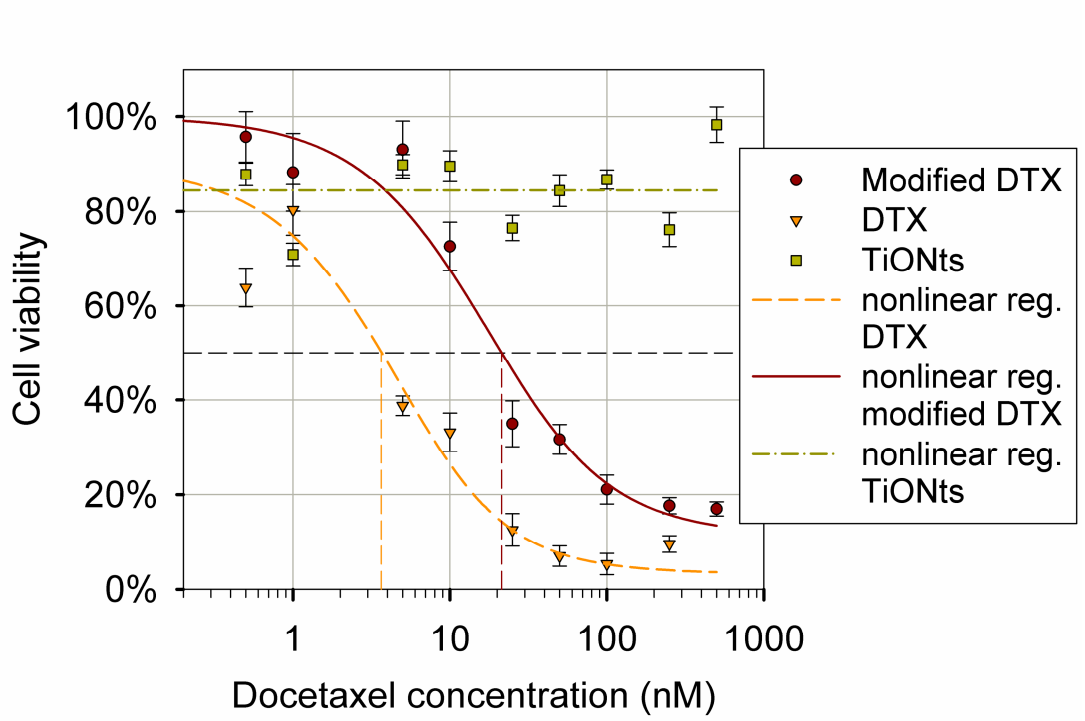

FIGURE 16.19
MTS cytotoxicity test results on PC3 cell lines showed 4 nM IC50 for docetaxel drug (orange dashed line), the absence of cytotoxicity for surface-modified TiONts (green dashed-dotted line) and intermediate toxicity for modified-docetaxel (dark red line)

To the best of our knowledge, no TiONt-based chemotherapy treatment has been yet developed and as a consequence it represents a novel and innovative way to deliver such a chemotherapy drug by increasing its load on TiONts and potentially reducing undesired side-effects. In the current study TiONts-docetaxel nanohybrids were engineered for intratumoral injections so that a maximum docetaxel payload could be delivered into the tumor but a systemic injection could be considered after the nanohybrids are modified by a targeting molecule. Detailed results are to be published in a dedicated communication [88].

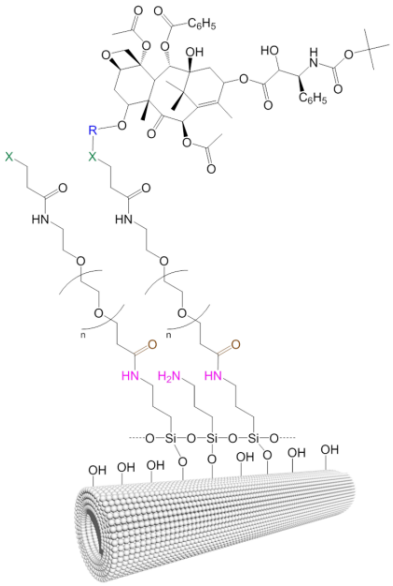

FIGURE 16.20
Grafting strategy for docetaxel-modified TiONTs: once PEGs are tethered on TiONTs–NH_2 *via* a peptide coupling, docetaxel molecules are then grafted on PEG function X *via* a linker R

Photodynamic therapy by phthalocyanine-grafted TiONTs

The phthalocyanine molecule described in paragraph 3.1 is not only capable of optical imaging but also to undergo intersystem crossing with oxygen to produce highly cytotoxic singlet oxygen upon absorption of light.
The grafting of zinc phthalocyanines is almost quantitatively realized *via* a click chemistry reaction (cf. 1,4-triazole cycloaddition on Figure 16.21) as was already achieved on iron oxide nanoparticules [43]. In this manner TiONTs could act as bimodal therapeutic composites but studies are still in progress on this promising aspect.
From the photodynamic therapy (PDT) point of view, zinc phthalocyanines (ZnPc) are of great interest [80]. PDT implies light, oxygen and the presence of a photosensitizing compound. This combination forms reactive species causing oxidation reaction within cell leading to necrosis. Phthalocyanines can be used as photosensitizers as well as porphyrin macrocycles already used *in vivo* for PDT applications because they have a high singlet oxygen quantum yield (*e.g.* Φ_Δ(ZnPc) = 0.50 in DMSO as a comparison to unchelated phthalocyanines $\Phi_\Delta(H_2Pc)$ = 0.14 in the same solvent or tetraphenylporphyrin Φ_Δ = 0.55 in chloroform).

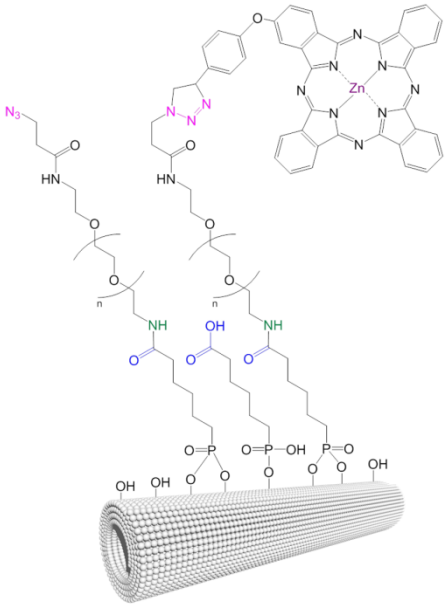

FIGURE 16.21
Grafting way of phthalocyanine-functionalized TiONts: carbonyl-functionalized phosphonate derivatives are condensed on TiONts, amino-PEG undergo peptide coupling on the latters and click chemistry is finally realized between alkyne-phthalocyanines and azide-PEG-TiONts

In addition the wavelength of the light source must be correctly selected to the photosensitizer excitation wavelength to produce oxygen reactive species. From this standpoint, phthalocyanines appear to have a more appropriate absorption wavelength than the porphyrins of the same metal chelate $\boldsymbol{\lambda_{emission}}$**(max, ZnPc)** (cf. Figure 16.13) to be compared to $\boldsymbol{\lambda_{emission}}$**(max, ZnPorphyrin)**) [81] with respect to the optimum *in vivo* optical window (650-1450 nm) [46].
Phthalocyanine-grafted TiONts present two major interests: on the one hand zinc phthalocyanine is capable of *in vivo* photodynamic therapy and on the other hand TiONts are themselves prone to increase the radiosensitizing effect. Eventually they can be used for bimodal therapeutic applications.

Conclusion

As a conclusion, the development of a TiONt-based nanomedicine is of great interest: the parameters of their synthesis are from now on known and set [5]. They are needle-shaped, *ca*. 150 nm long and have about a 10 nm diameter. More importantly, TiONt surface can be tuned by surface modification (silanization or phosphonatation for example) so that they become more stable in suspension (a mandatory prerequisite to any biomedical application) and ready for the grafting of molecules of interest one after the others. This step-by-step scaffold allows the development of a thoroughly characterized versatile platform.
Moreover surface-modified TiONts belong to the theranostic nanomaterial class [82-85] and appear as a potent tool, as recently shown in this chapter, that combine therapeutic aspects (enhanced radiotherapeutic treatment by radiosensitizing TiONts [8], nanocarrier for DNA transfection by PEI

coating [7] chemotherapy by grafting of taxane derivatives [86], or photodynamic therapy thanks to phthalocyanines [87]) as well as imaging ones (MRI probe [9], optical imaging probe [87], nuclear imaging probe [88]).
Future prospects will underscore efficacy and safety: TiONts can affect a wide range of diseases by improving both parameters, prolonging circulation time, and enhancing delivery specificity. Indeed safety is of paramount importance in any drug's translational roadmap [39]. Preliminary toxicity tests have been performed on TiONt nanohybrids at the different stages of elaboration but careful and exhaustive cytotoxicity, genotoxicity and other nanotoxicological tests would be an essential step [89] to evaluate the possibility of future clinical translation of these titanate nanotubes. According to the studies conducted in recent years, the authors are confident in the future relevance of a TiONt-based nanomedicine.

Acknowledgements

All the people who contributed in the results presented in this chapter are greatly acknowledged: Richard Decréau, Yann Bernhard, Céline Mirjolet, Bertrand Collin, Alexandra Oudot, Laure Dumond, David Vandroux, Mathieu Moreau, Claire Bernhard, Paul Walker, Thomas Gautier, Renée Mayap Talom, Olivier Heintz and Rémi Chassagnon as well as all the people from the IMAPPI program, the Pharm*Image*® consortium and the 3MIM agreement who are involved but not mentioned in the presented results.

References

1. T. Sekino, in Inorganic and metallic nanotubular materials: Recent technologies and applications, 17, (Springer-Verlag Berlin, Berlin, 2010).
2. T. Kasuga, M. Hiramatsu, A. Hoson, T. Sekino, K. Niihara, Langmuir, 14, 3160 (1998).
3. L. Niu, M. Shao, S. Wang, L. Lu, H. Gao, J. Wang, J. Mater. Sci., 43, 1510 (2008).
4. H. Niu, Y. Cai, J. Nanopart. Res., 39 (2011).
5. A.-L. Papa, N. Millot, L. Saviot, R. Chassagnon, O. Heintz, J. Phys. Chem. C, 113, 12682 (2009).
6. D.L. Morgan, H.-Y. Zhu, R.L. Frost, E.R. Waclawik, Chem. Mater., 20, 3800 (2008).
7. A.L. Papa, L. Dumont, D. Vandroux, N. Millot, Nanotoxicology, 7, 1131 (2013).
8. C. Mirjolet, A.L. Papa, G. Créhange, O. Raguin, C. Seignez, C. Paul, G. Truc, P. Maingon, N. Millot, Radiother. Oncol., 108, 136 (2013).
9. A.-L. Papa, L. Maurizi, D. Vandroux, P. Walker, N. Millot, J. Phys. Chem. C, 115, 19012 (2011).
10. D. Gong, C.A. Grimes, O.K. Varghese, W.C. Hu, R.S. Singh, Z. Chen, E.C. Dickey, J. Mater. Res., 16, 3331 (2001).
11. P. Roy, S. Berger, P. Schmuki, Angew. Chem. Int. Ed., 50, 2904 (2011).
12. T. Hashishin, K. Misawa, K. Kojima, C. Yogi, J. Tamaki, Int. J. Electrochem., 656939 (2011).
13. C. Yao, T.J. Webster, Journal of Biomedical Materials Research Part B: Applied Biomaterials, 91B, 587 (2009).
14. R.A. Petros, J.M. DeSimone, Nat. Rev. Drug Discov., 9, 615 (2010).
15. Q. Chen, W.Z. Zhou, G.H. Du, L.M. Peng, Adv. Mater., 14, 1208 (2002).
16. Y. Lan, X.P. Gao, H.Y. Zhu, Z.F. Zheng, T.Y. Yan, F. Wu, S.P. Ringer, D.Y. Song, Adv. Funct. Mater., 15, 1310 (2005).

17. C.K. Lee, C.C. Wang, M.D. Lyu, L.C. Juang, S.S. Liu, S.H. Hung, J. Colloid Interface Sci., 316, 562 (2007).
18. D. Wu, J. Liu, X.N. Zhao, A.D. Li, Y.F. Chen, N.B. Ming, Chem. Mater., 18, 547 (2006).
19. Y.T. Ma, Y. Lin, X.R. Xiao, X.W. Zhou, X.P. Li, Mater. Res. Bull., 41, 237 (2006).
20. A. Thorne, A. Kruth, D. Tunstall, J.T.S. Irvine, W.Z. Zhou, J. Phys. Chem. B, 109, 5439 (2005).
21. D.V. Bavykin, F.C. Walsh, European Journal of Inorganic Chemistry, 977 (2009).
22. M.S. Yilmaz, S. Kasap, S. Piskin, J. Therm. Anal. Calorim., 112, 1325 (2013).
23. M.D. Hernandez-Alonso, S. Garcia-Rodriguez, B. Sanchez, J.M. Coronado, Nanoscale, 3, 2233 (2011).
24. G.H. Du, Q. Chen, R.C. Che, Z.Y. Yuan, L.M. Peng, Applied Physics Letters, 79, 3702 (2001).
25. C.C. Tsai, H.S. Teng, Chem. Mater., 18, 367 (2006).
26. E. Morgado, M.A.S. de Abreu, G.T. Moure, B.A. Marinkovic, P.M. Jardim, A.S. Araujo, Mater. Res. Bull., 42, 1748 (2007).
27. D.V. Bavykin, V.N. Parmon, A.A. Lapkin, F.C. Walsh, J. Mater. Chem., 14, 3370 (2004).
28. J.J. Yang, Z.S. Jin, X.D. Wang, W. Li, J.W. Zhang, S.L. Zhang, X.Y. Guo, Z.J. Zhang, Dalton Transactions, 3898 (2003).
29. S. Zhang, L.M. Peng, Q. Chen, G.H. Du, G. Dawson, W.Z. Zhou, Physical Review Letters, 91, (2003).
30. D.L. Morgan, G. Triani, M.G. Blackford, N.A. Raftery, R.L. Frost, E.R. Waclawik, J. Mater. Sci., 46, 548 (2011).
31. D.V. Bavykin, J.M. Friedrich, F.C. Walsh, Adv. Mater., 18, 2807 (2006).
32. D.V. Bavykin, F.C. Walsh. *Titanate and titania nanotubes: Synthesis, properties and applications*. Cambridge, UK: RSC Publishing; 2010.
33. E. Morgado, M.A.S. de Abreu, O.R.C. Pravia, B.A. Marinkovic, P.M. Jardim, F.C. Rizzo, A.S. Araujo, Solid State Sciences, 8, 888 (2006).
34. Q. Chen, W. Zhou, G.H. Du, L.M. Peng, Adv. Mater., 14, 1208 (2002).
35. A.-L. Papa, V. Bellat, J. Boudon, H. Bisht, F. Sallem, R. Chassagnon, V. Bérard, N. Millot, Submitted, (2014).
36. Z.Q. Shi, X.P. Gao, D.Y. Song, Y.F. Zhou, D.Y. Yan, Polymer, 48, 7516 (2007).
37. Z.Y. Yuan, B.L. Su, Colloids and Surfaces a-Physicochemical and Engineering Aspects, 241, 173 (2004).
38. D.-E. Lee, H. Koo, I.-C. Sun, J.H. Ryu, K. Kim, I.C. Kwon, Chem. Soc. Rev., 41, 2656 (2012).
39. E.K.-H. Chow, D. Ho, Science Translational Medicine, 5, 216rv4 (2013).
40. I. Brnardić, M. Huskić, P. Umek, A. Fina, T.H. Grgurić, physica status solidi (a), 210, 2284 (2013).
41. M. Huskic, T.H. Grguric, P. Umek, I. Brnardic, Polym. Compos., 34, 1382 (2013).
42. Y.-Y. Song, H. Hildebrand, P. Schmuki, Surf. Sci., 604, 346 (2010).
43. J. Boudon, J. Paris, Y. Bernhard, E. Popova, R.A. Decreau, N. Millot, Chem. Commun., 49, 7394 (2013).
44. M. Yamaura, R.L. Camilo, L.C. Sampaio, M.A. Macêdo, M. Nakamura, H.E. Toma, J. Magn. Magn. Mater., 279, 210 (2004).
45. G. Guerrero, J.G. Alauzun, M. Granier, D. Laurencin, P.H. Mutin, Dalton Transactions, (2013).
46. V.J. Pansare, S. Hejazi, W.J. Faenza, R.K. Prud'homme, Chem. Mater., 24, 812 (2012).
47. H. Gu, K. Xu, Z. Yang, C.K. Chang, B. Xu, Chem. Commun., 4270 (2005).
48. L. Maurizi, H. Bisht, F. Bouyer, N. Millot, Langmuir, 25, 8857 (2009).
49. L. Maurizi, F. Bouyer, J. Paris, F. Demoisson, L. Saviot, N. Millot, Chem. Commun., 47, (2011).

50. S. Srivastava, R. Awasthi, D. Tripathi, M.K. Rai, V. Agarwal, V. Agrawal, N.S. Gajbhiye, R.K. Gupta, Small, 8, 1099 (2012).
51. K.S. Brammer, C.J. Frandsen, S. Jin, Trends Biotechnol., 30, 315 (2012).
52. S. Kubota, K. Johkura, K. Asanuma, Y. Okouchi, N. Ogiwara, K. Sasaki, T. Kasuga, J. Mater. Sci., 15, 1031 (2004).
53. S. Mahshid, C. Li, S.S. Mahshid, M. Askari, A. Dolati, L. Yang, S. Luo, Q. Cai, Analyst, 136, 2322 (2011).
54. R. Moumita, C. Sriparna, D. Tanmay, B. Somnath, A. Pushan, M. Shyamalava, Nanotechnology, 22, 415705 (2011).
55. K.T. Butterworth, S.J. McMahon, F.J. Currell, K.M. Prise, Nanoscale, 4, 4830 (2012).
56. A.Z. Wang, K. Yuet, L. Zhang, F.X. Gu, M. Huynh-Le, A.F. Radovic-Moreno, P.W. Kantoff, N.H. Bander, R. Langer, O.C. Farokhzad, Nanomedicine (Lond), 5, 361 (2010).
57. E. Porcel, S. Liehn, H. Remita, N. Usami, K. Kobayashi, Y. Furusawa, C. Le Sech, S. Lacombe, Nanotechnology, 21, 85103 (2010).
58. G. Le Duc, I. Miladi, C. Alric, P. Mowat, E. Brauer-Krisch, A. Bouchet, E. Khalil, C. Billotey, M. Janier, F. Lux, T. Epicier, P. Perriat, S. Roux, O. Tillement, ACS nano, 5, 9566 (2011).
59. R. Xu, J. Ma, X. Sun, Z. Chen, X. Jiang, Z. Guo, L. Huang, Y. Li, M. Wang, C. Wang, J. Liu, X. Fan, J. Gu, X. Chen, Y. Zhang, N. Gu, Cell Res., 19, 1031 (2009).
60. O.A. Sedelnikova, C.E. Redon, J.S. Dickey, A.J. Nakamura, A.G. Georgakilas, W.M. Bonner, Mutat. Res., 704, 152 (2010).
61. C. Wong, T. Stylianopoulos, J. Cui, J. Martin, V.P. Chauhan, W. Jiang, Z. Popovic, R.K. Jain, M.G. Bawendi, D. Fukumura, Proc Natl Acad Sci U S A, 108, 2426 (2011).
62. H. Maeda, Cancer Sci., 104, 779 (2013).
63. Y.-L. Wu, N. Putcha, K.W. Ng, D. Tai Leong, C.T. Lim, S.C.J. Loo, X. Chen, Acc. Chem. Res., 46, 782 (2012).
64. H. Summers, Nat Nano, 7, 9 (2012).
65. M. Mahmoudi, K. Azadmanesh, M.A. Shokrgozar, W.S. Journeay, S. Laurent, Chem. Rev., 111, 3407 (2011).
66. T.-G. Iversen, T. Skotland, K. Sandvig, Nano Today, 6, 176 (2011).
67. T. dos Santos, J. Varela, I. Lynch, A. Salvati, K.A. Dawson, Small, n/a (2011).
68. A. Verma, F. Stellacci, Small, 6, 12 (2010).
69. A.M. Studer, L.K. Limbach, L. Van Duc, F. Krumeich, E.K. Athanassiou, L.C. Gerber, H. Moch, W.J. Stark, Toxicol. Lett., 197, 169 (2010).
70. M.A. Maurer-Jones, Y.-S. Lin, C.L. Haynes, ACS nano, 4, 3363 (2010).
71. V. Mailänder, K. Landfester, Biomacromolecules, 10, 2379 (2009).
72. J. Gao, B. Xu, Nano Today, 4, 37 (2009).
73. S.E.A. Gratton, P.A. Ropp, P.D. Pohlhaus, J.C. Luft, V.J. Madden, M.E. Napier, J.M. DeSimone, Proceedings of the National Academy of Sciences, 105, 11613 (2008).
74. P.V. AshaRani, G. Low Kah Mun, M.P. Hande, S. Valiyaveettil, ACS nano, 3, 279 (2009).
75. S.J. Soenen, J. Demeester, S.C. De Smedt, K. Braeckmans, Nano Today, 8, 121 (2013).
76. K. Takakura, Acta Oncol, 35, 883 (1996).
77. H. Maezawa, Y. Furusawa, K. Kobayashi, K. Hieda, M. Suzuki, N. Usami, A. Yokoya, T. Mori, Acta Oncol, 35, 889 (1996).
78. P. Kolhar, N. Doshi, S. Mitragotri, Small, 7, 2094 (2011).
79. I. Koturbash, R.E. Rugo, C.A. Hendricks, J. Loree, B. Thibault, K. Kutanzi, I. Pogribny, J.C. Yanch, B.P. Engelward, O. Kovalchuk, Oncogene, 25, 4267 (2006).

80. C. Hadjur, G. Wagnières, F. Ihringer, P. Monnier, H. van den Bergh, J. Photochem. Photobiol. B: Biol., 38, 196 (1997).
81. M. Uttamlal, A. Sheila Holmes-Smith, Chem. Phys. Lett., 454, 223 (2008).
82. Y. Xing, J.H. Zhao, P.S. Conti, K. Chen, Theranostics, 4, 290 (2014).
83. S.S. Kelkar, T.M. Reineke, Bioconjugate Chem., 22, 1879 (2011).
84. H. Koo, M.S. Huh, I.-C. Sun, S.H. Yuk, K. Choi, K. Kim, I.C. Kwon, Acc. Chem. Res., 44, 1018 (2011).
85. Y. Saibi, V. Bellat, I. Séverin, J. Boudon, M.-C. Chagnon, N. Millot, Submitted, (2014).
86. J. Boudon, C. Mirjolet, A. Loiseau, T. Gautier, G. Créhange, N. Millot, To be submitted, (2014).
87. J. Paris, Y. Bernhard, J. Boudon, O. Heintz, R. Decréau, N. Millot, Submitted, (2014).
88. R. Mayap Talom, J. Paris, J. Boudon, M. Mathieu, C. Bernhard, A. Courteau, J.-M. Vrigneaud, A. Oudot, B. Collin, O. Heintz, F. Denat, N. Millot, Submitted, (2014).
89. P.P. Fu, Q. Xia, H.-M. Hwang, P.C. Ray, H. Yu, J. Food Drug Anal., 22, 64 (2014).